Chromenopyridine Drugs – Characterization and Reactions with Metal Complexes

By Phoebus Sun Cao

Spring 2017

Thesis submitted in completion of Honors Senior Capstone requirements for the DePaul University Honors Program

Dr. Kyle A. Grice, Department of Chemistry

Dr. Caitlin E. Karver, Department of Chemistry

Table of Contents

Abstract

The development of metal-based drugs using platinum and gold with chromenopyridine ligands was explored. A library of previously synthesized chromenopyridine compounds were characterized using ^{1}H nuclear magnetic resonance (NMR), ^{13}C NMR, UV-Vis, and fluorescence spectroscopies as well as x-ray crystallography, elemental analysis, and high resolution mass spectrometry (HRMS). Attempted complexation reactions between the chromenopyridines and platinum(II) or gold(I) generated a carbocation species. The carbocation was isolated and characterized by ^{1}H NMR spectroscopy and x-ray crystallography. This indicates that C–S bond cleavage is the mode of reactivity between metals such as platinum and gold and the chromenopyridine compounds. The characterization and behavior of these compounds were also supported using density functional theory (DFT) studies.

Introduction

Liver fibrosis is a critical wound-healing response to chronic liver injury such as hepatitis C virus (HCV).[1] Fibrosis involves the formation of excessive scar tissue during wound healing, and is associated with inflammation. If persistent, liver fibrosis can lead to cirrhosis and hepatocellular carcinoma (HCC), a form of liver cancer. Hence, the identification of novel anti-fibrotic compounds can provide opportunities for the intervention and treatment of HCV-mediated liver cancer and similar diseases. However, developing treatments for cancer and chronic liver diseases associated with HCV remains a challenge. For HCC caused by HCV, a recent advancement was the approval of the drug sorafenib for the treatment of unresectable tumors in the liver, but significant work is still needed in the field.[2] One approach that is attractive is the use of metal-based drugs, which offer novel geometries and reactivities compared to organic compounds.[3]

Organic compounds are generally defined as molecules featuring carbon and hydrogen atoms, with some other heteroatoms such as oxygen, nitrogen, sulfur, and chlorine sometimes present. Carbon atoms can bind up to four other atoms in a defined set of geometries. The defined geometries found within organic compounds are tetrahedral, trigonal planar, and linear, which possess idealized bond angles of 109.5°, 120°,

and 180°, respectively. This set of geometries helps enable structural understanding in organic chemistry because changes in bond angles and lengths indicate changes in bond character between atoms. Ultimately, however, relying on organic chemistry alone can limit the structures that can be developed for drug molecules. For instance, binding interactions between an organic drug structure and an enzyme might not be optimal because of the available geometries of the carbons. Compounds that feature metal centers can offer different structures, with angles such as 90° in octahedral or square planar complexes. Also, drugs with metal centers can sometimes bind to more atoms than carbon (up to six different atoms), providing additional potentially reactive groups. Another benefit of metals is that they cannot be metabolized to CO_2 like organic molecules and therefore may be more persistent and effective drugs *in vivo*. For these reasons, metal-based drugs can offer new opportunities in therapeutic structures that would generally be very difficult or impossible to accomplish with organic compounds.

Despite their potential, there is limited work on the development of metal-based drugs for diseases other than cancer. Within cancer there are notable examples of successful metal-based drugs including cisplatin, a commonly-used and effective chemotherapy agent that is based on a platinum(II) metal complex.[4] Moreover, metal-based drugs for cancer, such as cisplatin, carboplatin, and oxaliplatin, tend to be more effective towards certain cancers than others, indicating cancer-type selectivity. Cisplatin, for example, as seen in Figure 1 below, is noted as being particularly effective against testicular cancer.[5]

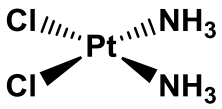

Figure 1: The structure of the square planar Pt(II) chemotherapy drug cisplatin.

For the reasons discussed above, the development of anti-fibrotic and/or anti-cancer agents for the liver based on metal-based drugs was appealing. The proposed novel approach in this project was a "double-warhead" method, wherein metal complexes featuring Pt(II) and Au(I), a platinum or gold metal center, could release an organic small molecule drug and act as drugs themselves, delivering two drugs as one

compound in a synergistic effect. To our knowledge, this approach has not been explored for the treatment of HCC, HCV, or similar liver diseases. This project focused on the synthesis of chromenopyridine metal complexes for use as potential anti-fibrotic/anti-cancer drugs and their reactions with metals to make the "double-warhead" compounds (Scheme 1).

Scheme 1: The general concept of the "Double Warhead" approach.

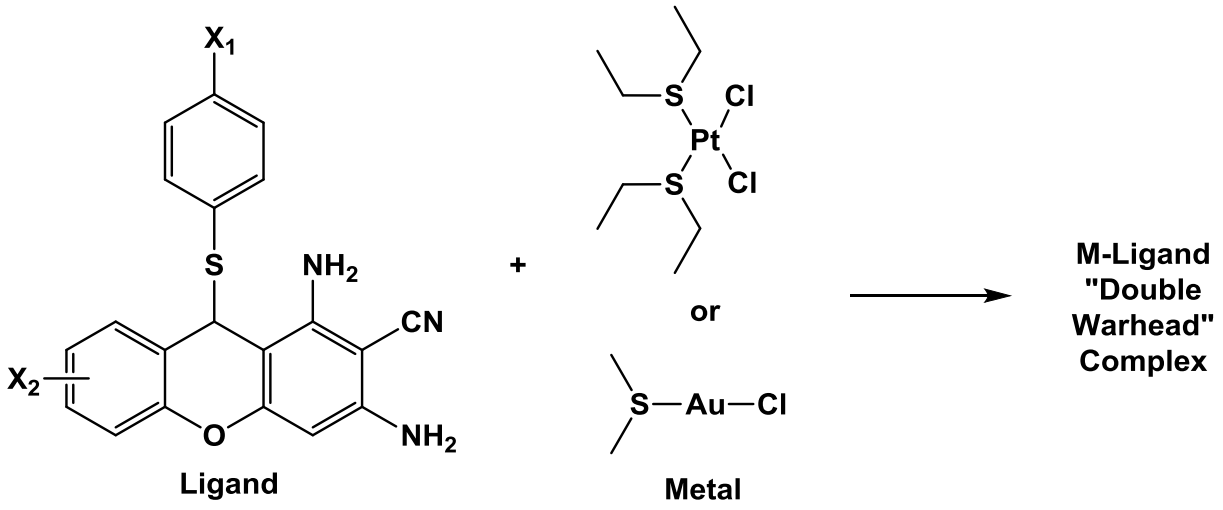

Key to this project was the complete characterization of the chromenopyridine compounds and their products. Characterization of the structural aspects of the chromenopyridine compounds was performed through a variety of methods including ^{1}H NMR (nuclear magnetic resonance), ^{13}C NMR, fluorescence and UV-Vis spectroscopies, as well as x-ray crystallography, elemental analysis, and high resolution mass spectrometry (HRMS). In addition, computational methods were utilized to study the chromenopyridine compounds. NMR spectroscopy was an ideal tool to analyze these compounds because hydrogen or carbons atoms on different parts of a molecule possess unique environments characterize the structural properties of each organic molecule. In a reaction, for instance, it is possible to observe changes through NMR spectroscopy as the environments of the hydrogen and carbon atoms in the molecules change. UV-Vis and fluorescence spectroscopies were used because the chromenopyridine compounds possess highly conjugated systems that render them both colorful and emissive. In UV-Vis spectroscopy, the

intensities of light absorption at various wavelengths are quantified. In fluorescence spectroscopy, the wavelengths of light emitted upon excitation of the compound are obtained. Substitutions in functional groups in a molecule featuring a highly conjugated system can significantly affect light absorption and emission resulting in different UV-Vis and fluorescence spectra between different compounds. X-ray crystallography allows for the determination of a structural model of the compound packing within a crystal, thus determining the overall geometry of the species in the solid state. Elemental analysis and high resolution mass spectrometry are used to assess the composition and purity of a material. The combination of these techniques results in the complete characterization of a compound, which is critical for drug molecules before they are examined in biological assays. The understanding of the structure allows for creation of structure-activity relationships (SARs) between the drug and the biological responses.

This project is a relatively new collaboration between Dr. Grice's lab at DePaul University and two research laboratories at the Rosalind Franklin University of Medicine and Science (RFUMS) in North Chicago, Illinois. Dr. Shivaputra Patil at RFUMS is a synthetic medicinal chemist. He synthesized the chromenopyridine compounds at RFUMS and isolated them as solids. These compounds were then sent to Dr. Grice's laboratory, where they were fully characterized by the methods described above, as well as reacted with metal complexes. Then the compounds were tested in biological assays at RFUMS in the laboratory of Dr. Gulam Waris, a molecular biologist specializing in the studying of liver fibrosis, hepatitis C virus, and related diseases. The results of the collaborative work are discussed below, with a focus on the research contributions of the author while in Dr. Grice's research laboratory.

Results and Discussion

A series of several chromenopyridines denoted SP-109 through SP-163 (27 total compounds, only odd numbers were used in the naming system) were synthesized at RFUMS by Dr. Shivaputra Patil's research group and sent to Dr. Grice's lab for analysis and reactions with metal complexes. The general structure of these molecules is shown in Figure 2, with some examples of the substituents on the molecules. The synthesis involved a multi-component reaction in one-pot, and the products were isolated without the need for chromatography as shown in Scheme 2.

Scheme 2. Syntheses of 5-arythio-5H-chromenopyridines using a multi-component reaction method.

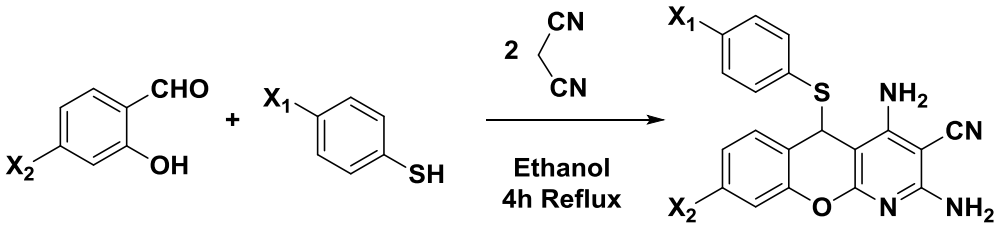

These chromenopyridine compounds share a common tricyclic core with a thiophenol group attached to the central carbon. They were characterized using ^{1}H NMR, ^{13}C NMR, UV-Vis, and fluorescence spectroscopies. In addition, samples were sent out for elemental analysis and high resolution mass spectrometry. Through these methods, the structure, purity, and spectroscopic behavior of these compounds were assessed.

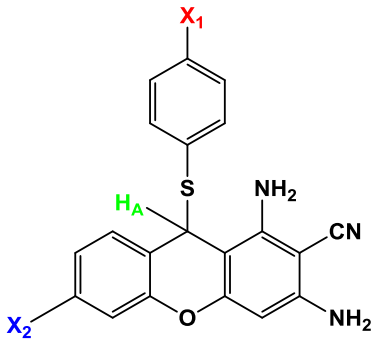

Figure 2: General structure of the chromenopyridine compounds synthesized at RFUMS, with some examples of the substituent groups on the molecules.

The ^{1}H NMR data for the complexes in DMSO-d_6 were consistent with their proposed structures. Key features in the ^{1}H NMR spectra included signals for the presence of a total of 8 aromatic protons that were consistent across all compounds. In addition, across all compounds, there was as a single proton significantly shifted downfield to 5.52-5.69 ppm, corresponding to the proton on the central carbon attached to the sulfur as seen, labelled as H_A, in Figure 3. The NH_2 groups were observed as broad singlets in the aromatic region. The integrations of the signals were consistent with the number of protons on the compounds, and the number of signals in the ^{13}C NMR spectra were consistent with the number of different carbon environments in the molecules.

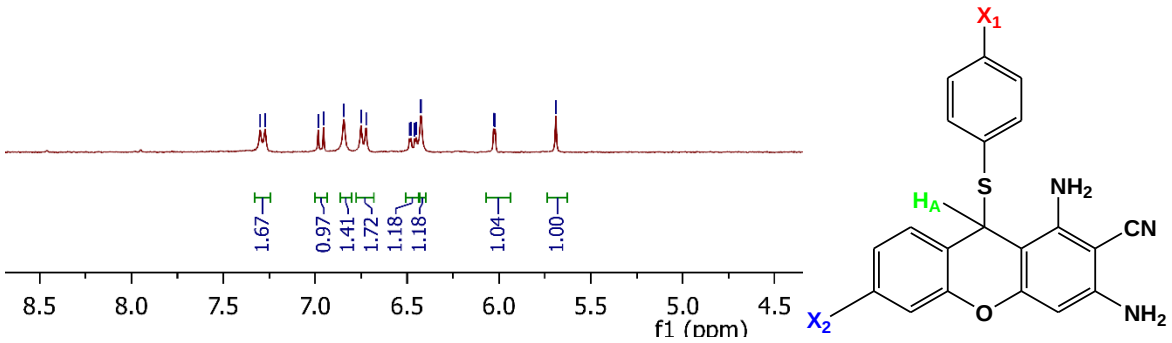

Figure 3: A partial ^{1}H NMR spectra of SP-111 collected in DMSO-d_6. The peak for the proton, labelled as H_A, was determined to be significantly downfield at 5.69 ppm for SP-111.

The compounds with the NEt_2 substitution at the X_2 position were observed to be red or pink powders while compounds with the OMe substitution at the X_2 position were observed to be pale yellow powers. These results were reflected in their UV-Vis spectra, which displayed significant differences in absorbance in the visible region, as seen in Figure 4.

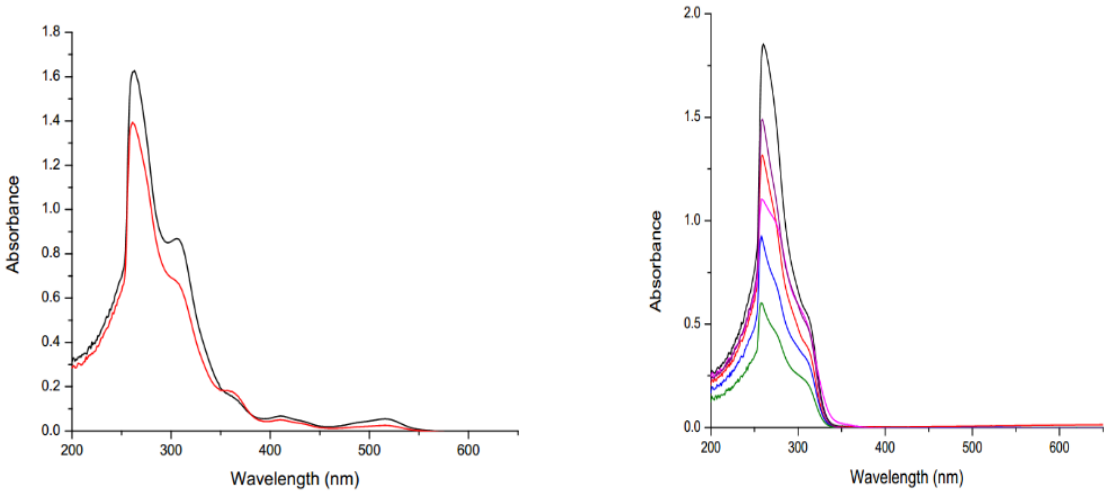

Figure 4: The left spectra displays the trend for the UV-Vis absorbance of NEt_2 substituted chromenopyridines (SP-109 and SP-113) while the right spectra displays the trend for UV-Vis absorbance of OMe substituted chromenopyridines (SP-123, SP-125, SP-127, SP-129, and SP-131). Substitutions were at the X_2 position of the chromenopyridine.

In general, the NEt_2-substituted chromenopyridines displayed some level of absorbance in the visible region whereas the OMe-substituted chromenopyridines did not. It is important to note that these spectra are not normalized in regards to concentration but were obtained simply to visualize differences in trends between the X_2-substituted chromenopyridines.

In order to assess the structure of the compounds, attempts were made to grow suitable crystals for X-ray crystallography. We were successful in growing crystals of SP-125, which were analyzed at the North Carolina State University Department of Chemistry X-ray Crystallography Facility. The molecular structure obtained from that sample is shown in Figure 5. Lower quality crystals were also obtained for SP-123 and SP-127. The data is not shown, but the structures are similar to SP-125.

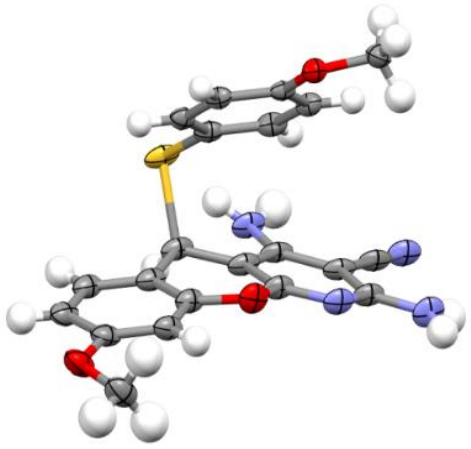

Figure 5: The x-ray crystallography structure of chromenopyridine compound SP-125 with ellipsoids at 50%. Crystals were obtained through vapor diffusion using dichloromethane (DCM) and pentane. The white atoms represent hydrogen, which were placed using a model and were not directly observed in the X-ray study. The grey atoms represent carbon atoms. The red atoms represent oxygen. The blue atoms represent nitrogen. The yellow atom represents sulfur.

While single crystals of most of the chromenopyridine compounds remained unobtainable despite multiple attempts (e.g. SP-109 though SP-121), there is a significant amount of similarity between the successfully crystallized compounds obtained through vapor diffusion (SP-123, SP-125, and SP-127). As a result, observations from these compounds can be generally applied to other chromenopyridine compounds. As can be seen in Figure 5, notable structural characteristics for the chromenopyridine compound included the thiophenol ring bent above the tricyclic core and the fact that the tricyclic core is puckered in the middle due to the presence of a sp^3 carbon center. The C-S-C bond angle between the tricyclic core and the thiophenol was observed to be 99.03°. In addition, the bond length between the central carbon and the sulfur was found to be 1.884 Å, as compared to an average C-S single bond length of 1.82 Å.[6] Within the tricyclic core, the C-N bonds on the aromatic system were found to be 1.341 and 1.343 Å. When compared to aniline, which has a C-N bond length of 1.431 Å, the C-N bond lengths are relatively shorter within the chromenopyridine.[7] With the structures of the molecules elucidated, their overall purity was assessed with elemental analysis in the form of determining % C, H, and N by mass in the samples of the chromenopyridines. The values obtained were in close agreement with the theoretical values for the %

composition, indicating that the bulk samples were relatively pure. For the chromenopyridines substituted at the X_2 position with a NEt_2 group, the values were predicted to be roughly 60% carbon, 4% hydrogen, and 14% nitrogen. However, substitutions at the X_1 position affect these percentages. The theoretical and experimental values are listed in the materials and methods sections.

Finally, HRMS data was collected for several of the compounds. HRMS can be used to confirm the molecular weight of a compound and thus its identity. It operates by ionizing a compound and measuring the mass to charge ratio. Surprisingly, the HRMS data for SP-109 though SP-121 all displayed the same major ion peak, and no parent ion, with a mass of 308.1504. This value is a smaller mass than any of the examined chromenopyridine compounds, which have masses in a range of 435.52 – 496.42, and it was puzzling that this would occur when the compounds had been characterized by multiple methods. This could indicate that all of the compounds fragment in the same manner and that there is a facile path for such fragmentation. This could be due to the formation of a carbocation that is common to all of the species (Figure 6).

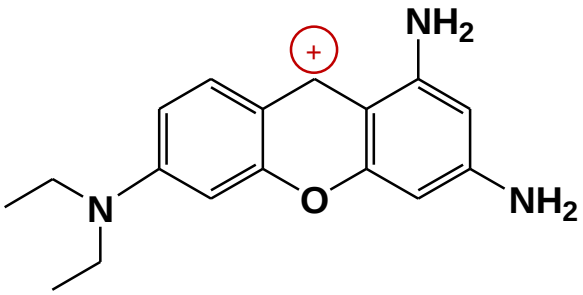

Figure 6: Proposed cation fragment for SP-109 through SP-121 according to HRMS data.

With the parent chromenopyridine compounds completely characterized, reactions between the chromenopyridines and various metal compounds were conducted in order to synthesize complexes that could act as "double-warheads". One of the first reactions attempted involved combining SP-115 and $(SEt_2)_2PtCl_2$ in dichloromethane. $(SEt_2)_2PtCl_2$ is a source of "$Pt(II)Cl_2$" that is soluble in polar organic solvents. Preliminary ^1H NMR spectroscopy data of this reaction suggested that C−S bond cleavage had occurred, due to the absence of the thiophenol resonances in the ^1H NMR spectrum. The product was

crystallized via vapor diffusion using dimethylformamide and ether, and the crystals were analyzed by X-ray crystallography. The resulting structure demonstrated that the product of the reaction was an organic cation with a planar structure, in contrast with the puckered tricyclic core of the original chromenopyridine (Figure 7). Further studies reacting $(SEt_2)_2PtCl_2$ with SP-109 and SP-111 also suggested that C–S bond cleavage had occurred based on NMR spectroscopy. In each case, it appeared that the same tricyclic carbocation was formed based on the matching ^1H NMR spectrum signals in the reaction solutions. In addition, a reaction between SP-109 and $(SMe_2)AuCl$ in dichloromethane produced a similar ^1H NMR spectra to the platinum reactions and suggested C−S bond cleavage could be promoted by Au(I) as well.

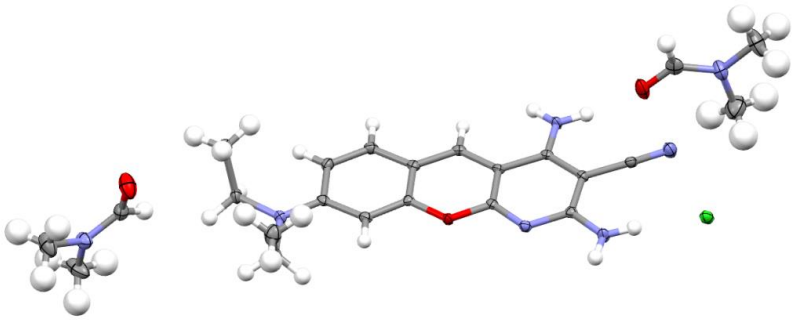

Figure 7: The x-ray crystallography structure of the cation product for the reaction of SP-115 and $(SEt_2)_2PtCl_2$ with ellipsoids shown at 50%. In the structure, the tricyclic core is planar. Crystals were obtained through vapor diffusion using dimethylformamide (DMF) and ether. The white atoms represent hydrogen. The grey atoms represent carbon atoms. The red atoms represent oxygen. The blue atoms represent nitrogen. The green atom represents chlorine.

From the crystal structure in Figure 7, it can be noted how the cation is stabilized by dimethylformamide molecules and a chloride ion. In addition, it was observed that the cation formed matched the structure proposed from the HRMS data. In regards to the stability of the cation product, it can be described as quite stable because it does not react with the chloride ion (a potential nucleophile) in solution. This is likely due to the highly delocalized positive charge in the cation.

To analyze the bond cleavage and to understand the chromenopyridine compounds in more detail, density functional theory (DFT) calculations were performed. A simplified version of the chromenopyridine compound, based on SP 113 (but with NMe_2 instead of NEt_2), was constructed and its geometry was

optimized at the B3LYP/6-31+G(d,p) level of theory. A similar calculation was performed with the corresponding carbocation fragment. From this output, the calculated molecular orbitals were examined. It was observed that the HOMO distribution was more delocalized across the compound for the carbocation than the starting chromenopyridine. A larger delocalization over the planar structure of the carbocation for these chromenopyridines likely contributes to the stability of the product and the weakened C−S bonds in the reactants as seen in Figure 8.

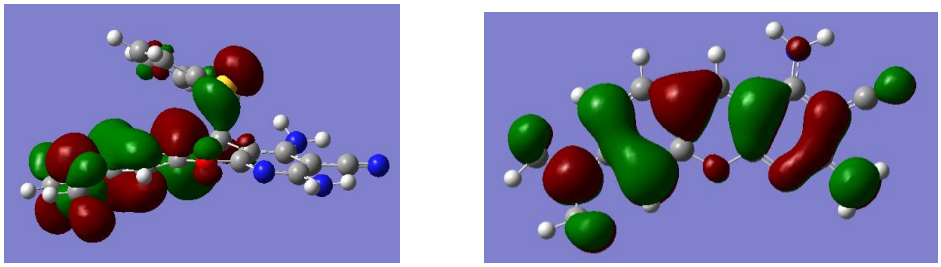

Figure 8: The HOMO diagrams for a simplified chromenopyridine, based on SP-113, (left) and a cation (right) demonstrating a more delocalized HOMO in cation form. Calculations utilized the B3LYP/6-31+G(d,p) level of theory.

In addition, time dependent (TD) DFT calculations were performed to determine if the UV-Vis spectra of the chromenopyridine compounds could be accurately predicted. Using the B3LYP/6-31+G(d,p) level of theory, calculations were performed on the structure of SP-125. When compared to experimentally obtained data, much of the predicted values were in close agreement (Figure 9).

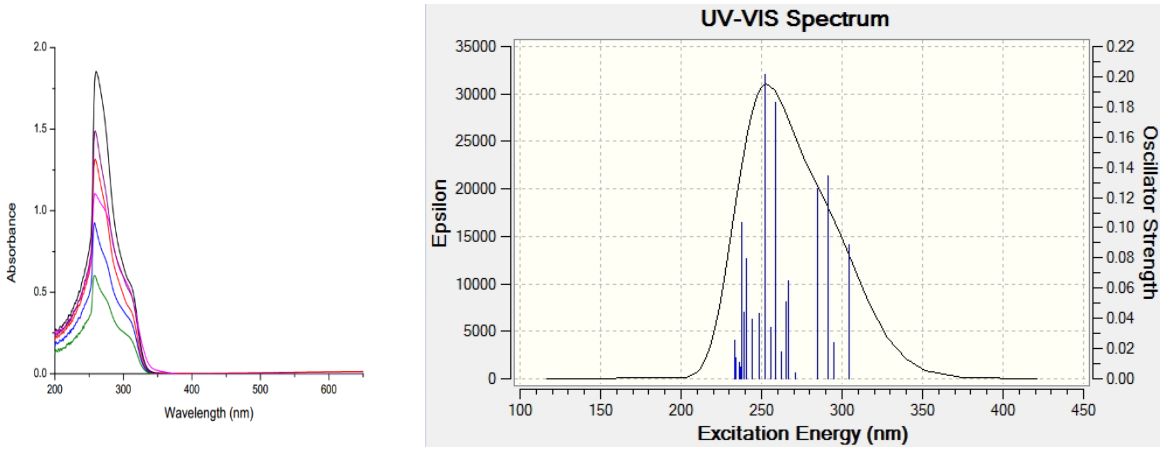

Figure 9: The experimentally obtained UV-Vis spectra of OMe substituted chromenopyridines (left) and a TD-DFT predicted UV-Vis spectra of SP-125 (right). Calculations utilized the B3LYP/6-31+G(d,p) level of theory.

Despite the lack of success with metal complexation, the chromenopyridine compounds showed promise with *in-vitro* studies on LX2 human hepatic stellate cells.[8] LX2 cells are a major fibrogenic cell type that contribute to the development of liver fibrosis and can be easily activated in a laboratory setting through culturing on uncoated plastic plates. Under these conditions, the cells spontaneously exhibit fibrosis, which can be inhibited by treatment with appropriate drug molecules. To examine anti-fibrotic potential, compounds SP-109 to SP-121 were tested at various concentrations. It was found that SP-111 and SP-115 both demonstrated inhibitory effects on liver cell fibrotic activation at 10 μM. This was determined through examining cell populations and the morphological aspects of the cells upon addition of the chromenopyridine compounds. Preliminary examinations, using Western-Blot methods, suggest that the drugs inhibit HCV nonstructural protein NS3. While additional studies are required, these results support the continued efficacy for using chromenopyridine compounds in drug development.

Conclusions and Future Directions

The chromenopyridine analogs were successfully characterized through a variety of spectroscopic methods such as ^{1}H NMR, ^{13}C NMR, UV-Vis, and fluorescence spectroscopies as well as high resolution mass spectrometry. In addition, elemental analysis was used to establish purity and a high-quality single crystal x-ray crystallography structure for one of the compounds was successfully obtained. The spectroscopic and structural data matched the expected connectivities of the compounds, indicating they were successfully synthesized.

For the attempted synthesis of chromenopyridine metal complexes, it was found that the chromenopyridine compounds underwent C–S bond cleavage upon reaction with platinum or gold compounds. These observations were supported by ^{1}H NMR spectroscopy, X-ray crystallography of the carbocation compound, and computational calculations. As a result, it appeared that the current chromenopyridines possessing the C–S bond are inappropriate for further studies with metals such as Pt(II) and Au(I). Future experiments for the synthesis of chromenopyridine metal complexes will address C – S bond issue. One possibility is the modification of the current compounds through reduction to eliminate the thiophenol group or through substitution of the thiophenol with a different functional group.

Materials and Methods

General Considerations

Unless otherwise stated, all chemicals were used as provided by their respective manufacturers. Chromenopyridine compounds were supplied from Dr. Shivaputra Patil's research group at RFUMS. All NMR spectra were collected using a Bruker AVANE 300 MHZ NMR spectrometer at room temperature. Spectra were internally referenced to residual solvent peaks and are reported downfield of tetramethysilane (TMS, $\delta = 0$). X-ray diffraction analyses were performed by the North Carolina State University Department of Chemistry X-ray Structural Facility. Pentane, acetonitrile (ACN), and dichloromethane were purified using an Innovative Technology PureSolv system under N_2. Elemental analyses were performed

by Midwest Microlabs, LLC. HRMS was collected at the University of Illinois Mass Spectrometry Lab in the School of Chemical Sciences (Urbana, IL). UV-Visible spectra were obtained on a Varian Cary 100 UV-Vis spectrometer. All of the species had large absorptions in the UV, and the λ values reported are for the lowest energy absorptions observed in the visible range. Fluorescence spectra were obtained on a Cary Eclipse Fluorescence Spectrophotometer by exciting at the lowest energy wavelength for each compound.

Characterization of SP-109

^{1}H NMR (300 MHz, DMSO-d_6): δ 7.16 (d, *J* = 9.0 Hz, 2H), 6.98 (d, *J* = 9.0 Hz, 1H), 6.78-6.84 (m, 4H), 6.48 (dd, *J* = 3.0 Hz, 1H), 6.42 (bs, 2H), 6.02 (d, *J* = 3.0 Hz, 1H), 5.68 (s, 1H), 3.32 (q, 4H merged with DMSO water peak), 1.07 (t, *J* = 6.0 and 9.0 Hz, 6H,); ^{13}C-NMR (DMSO-d_6, 75.4 MHz): δ 160.0, 159.5, 156.2, 152.3, 147.7, 137.6, 133.6, 130.6, 129.2, 128.0, 116.6, 108.2, 107.5, 97.5, 86.9, 70.1, 43.7, 12.2; UV-Vis (DMSO): λ_{max} = 516 nm; Fluorescence (DMSO): $\lambda_{emission}$ = 547 nm; HRMS (MeOH): Found: 308.1504, consistent with C-S cleavage. Anal. Calcd. ($C_{23}H_{22}ClN_5OS$): C, 61.12; H, 4.91; N, 15.50 Found: C, 60.52; H, 4.94; N, 15.57.

Characterization of SP-111

^{1}H NMR (300 MHz, DMSO-d_6): δ 7.29 (d, *J* = 9.0 Hz, 2H), 6.98 (d, *J* = 9.0 Hz, 1H), 6.84 (bs, 2H), 6.74 (d, *J* = 9.0 Hz, 2H), 6.44 (dd, *J* = 3.0 Hz, 1H), 6.42 (bs, 2H), 6.02 (d, *J* = 3.0 Hz, 1H), 5.69 (s, 1H), 3.32 (q, 4H merged with DMSO water peak), 1.07 (t, *J* = 6.0 and 9 Hz, 6H,); ^{13}C-NMR (DMSO-d_6, 75.4 MHz): δ 160.0, 159.6, 156.2, 152.3, 147.7, 137.8, 131.1, 130.9, 129.1, 122.3, 116.7, 108.2, 107.5, 97.4, 87.0, 70.1, 43.7, 12.2; UV-Vis (DMSO): λ_{max} = 516 nm; Fluorescence (DMSO): $\lambda_{emission}$ = 546 nm; HRMS (MeOH): Found: 308.1504, consistent with C-S cleavage; Anal. Calcd. ($C_{23}H_{22}BrN_5OS$): C, 55.65; H, 4.47; N, 14.11 Found: C, 55.59; H, 4.47; N, 14.23.

Characterization of SP-113

^{1}H NMR (300 MHz, DMSO-d_6): δ 6.95 (d, *J* = 6.0 Hz, 2H), 6.76 (bs, 2H), 6.65-6.68 (m, 3H), 6.46 (dd, *J* = 3.0 Hz, 1H), 6.35 (bs, 2H), 6.00 (d, *J* = 3.0 Hz, 1H), 5.52 (s, 1H), 3.66 (s, 3H), 3.32 (q, 4H merged with DMSO water peak), 1.07 (t, *J* = 6.0 Hz, 6H,); ^{13}C-NMR (DMSO-d_6, 75.4 MHz): 159.8, 159.7, 159.3, 156.2, 152.2, 147.6, 137.7, 129.3, 121.9, 116.6, 113.6, 108.1, 107.9, 97.6, 87.5, 70.1, 55.1, 43.7, 43.2, 12.4; UV-Vis (DMSO): λ_{max} = 516 nm; Fluorescence (DMSO): $\lambda_{emission}$ = 547 nm; HRMS (MeOH): Found: 308.1504, consistent with C-S cleavage.; Anal. Calcd. ($C_{24}H_{25}N_5O_2S$): C, 64.41; H, 5.63; N, 15.65 Found: C, 63.98; H, 5.49; N, 15.67.

Characterization of SP-115

^{1}H NMR (300 MHz, DMSO-d_6): δ 6.91-6.98 (m, 3H), 6.75-6.82 (m, 4H), 6.48 (dd, *J* = 3.0 Hz, 1H), 6.40 (bs, 2H), 6.01 (d, *J* = 3.0 Hz, 1H), 5.63 (s, 1H), 3.32 (q, 4H merged with DMSO water peak), 1.07 (t, *J* = 6.0 and 9.0 Hz, 6H,); ^{13}C-NMR (DMSO-d_6, 75.4 MHz): 164.3, 161.1, 160.0, 159.5, 156.2, 152.2, 147.7, 138.4, 129.3, 127.1, 116.7, 115.2, 114.9, 108.2, 107.6, 97.4, 87.0, 70.1, 43.8, 12.3 ppm ; ^{19}F NMR (DMSO-d_6, 282.4 MHz): -110.6; UV-Vis (DMSO): λ_{max} = 514 nm; Fluorescence (DMSO): $\lambda_{emission}$ = 541 nm; HRMS (MeOH): Found: 308.1504, consistent with C-S cleavage ; Anal. Calcd. For $C_{23}H_{22}FN_5OS$: C, 63.43 ; H, 5.09 ; N, 16.08 Found: C, 63.21; H, 5.08 ; N, 16.17. HRMS only

Attempted Synthesis of SP-115-$PtCl_2$

To a solution of chromenopyridine SP-115 (30.2 mg, 0.0693 mmol) in 8 mL of DCM, $Pt(SEt_2)_2Cl_2$ (32.0 mg, 0.0717 mmol) was added and the solution was allowed to stir for several days. After rotary evaporation to remove the solvent and rinsing with ether, 21.8 mg of product was collected. Vapor diffusion was utilized with DMF and ether as solvents to form a red crystalline precipitate and crystals suitable for X-ray crystallography. Yield: 44.8% ^{1}H NMR (300 MHz, DMSO-d_6): δ 6.91-6.98 (m, 3H), 6.75-6.82 (m, 4H), 6.48 (dd, *J* = 3.0 Hz, 1H), 6.40 (bs, 2H), 6.01 (d, *J* = 3.0 Hz, 1H), 5.63 (s, 1H), 3.32 (q, 4H merged with DMSO water peak), 1.07 (t, *J* = 6.0 and 9.0 Hz, 6H).

Attempted Synthesis of SP-109-AuCl

To a solution of chromenopyridine SP-109 (12.7 mg, 0.0281 mmol) in 7 mL of DCM, $(SMe_2)AuCl$ (8.3 mg, 0.028 mmol) was added and the solution was allowed to stir for few days. After rotary evaporation to remove the solvent, the solid was subjected to vapor diffusion using DMF and ether as solvents. In another vial, vapor diffusion was set up using DMF and MeOH as solvents. No crystals formed in either case. ^{1}H NMR data was obtained in DMSO-d_6 and was found to match the signals observed for SP-115-$PtCl_2$.

^{1}H NMR Spectroscopy Analysis for Chromenopyridine Carbocation

With use of deuterated acetonitrile, chromenopyridine SP-109 and SP-111 were dissolved with $Pt(SEt_2)_2Cl_2$ in separate NMR tubes. After collecting initial ^{1}H NMR spectra, a few drops of D_2O was added. Afterwards, the contents of both NMR tubes were combined into one tube to see if the carbocation product from each reaction resulted in overlaying peaks. ^{1}H NMR data was obtained in DMSO-d_6 and was found to match the peaks observed for SP-115-$PtCl_2$.

Density Functional Theory (DFT) Calculations

Density functional theory (DFT) calculations were performed using the *Gaussian 09* software package.[9] Input files and output files were processed using *GaussView*.[10] All calculations were performed with the B3LYP hybrid functional[11], which includes Becke's exchange-correlation functional[12], the Lee-Yang-Parr 1988 correlation functional[13], and the Vosko, Wilk, and Nusair Local Spin Density correlation.[14] Chromenpyridine structures were optimized using the 6-31+G(d,p) basis set[15]. All structures were optimized to minima based on the use of frequency calculations to determine that they did not possess any imaginary frequencies. If imaginary frequencies were found, the structure was adjusted along those vectors and was re-optimized, and this process was repeated until no imaginary frequencies were found.

X-Ray Crystallography Information

For SP-125, a pale yellow plate-like specimen of $C_{20}H_{15}FN_4O_2S$, approximate dimensions 0.040 mm x 0.224 mm x 0.288 mm, was used for the X-ray crystallographic analysis. The X-ray intensity data were measured. The total exposure time was 13.32 hours. The frames were integrated with the Bruker SAINT software package using a narrow-frame algorithm. The integration of the data using a monoclinic unit cell yielded a total of 34880 reflections to a maximum θ angle of 30.51° (0.70 Å resolution), of which 5533 were independent (average redundancy 6.304, completeness = 99.9%, R_{int} = 3.53%, R_{sig} = 2.92%) and 4391 (79.36%) were greater than $2\sigma(F^2)$. The final cell constants of a = 14.6027(7) Å, b = 7.1994(4) Å, c = 18.1327(10) Å, β = 107.694(2)°, volume = 1816.12(17) $Å^3$, are based upon the refinement of the XYZ-centroids of 9859 reflections above 20 σ(I) with 4.715° < 2θ < 62.87°. Data were corrected for absorption effects using the Multi-Scan method (SADABS). The ratio of minimum to maximum apparent transmission was 0.955. The calculated minimum and maximum transmission coefficients (based on crystal size) are 0.9410 and 0.9920. The final anisotropic full-matrix least-squares refinement on F^2 with 270 variables converged at R1 = 3.77%, for the observed data and wR2 = 10.18% for all data. The goodness-of-fit was 1.025. The largest peak in the final difference electron density synthesis was 0.415 $e^-/Å^3$ and the largest hole was -0.249 $e^-/Å^3$ with an RMS deviation of 0.056 $e^-/Å^3$. On the basis of the final model, the calculated density was 1.443 g/cm^3 and F(000), 816 e^-.

Table 1. Sample and crystal data for SP-125.

Identification code	SP-125	
Chemical formula	$C_{20}H_{15}FN_4O_2S$	
Formula weight	394.42 g/mol	
Temperature	100(2) K	
Wavelength	0.71073 Å	
Crystal size	0.040 x 0.224 x 0.288 mm	
Crystal habit	pale yellow plate	
Crystal system	monoclinic	
Space group	P 1 21/n 1	
Unit cell dimensions	a = 14.6027(7) Å	α = 90°
	b = 7.1994(4) Å	β = 107.694(2)°
	c = 18.1327(10) Å	γ = 90°
Volume	1816.12(17) $Å^3$	
Z	4	
Density (calculated)	1.443 g/cm^3	
Absorption coefficient	0.213 mm^{-1}	
F(000)	816	

Table 2. Data collection and structure refinement for SP-125

Theta range for data collection	2.14 to 30.51°
Index ranges	-19<=h<=20, -10<=k<=10, -23<=l<=25
Reflections collected	34880
Independent reflections	5533 [R(int) = 0.0353]
Coverage of independent reflections	99.9%
Absorption correction	Multi-Scan
Max. and min. transmission	0.9920 and 0.9410
Refinement method	Full-matrix least-squares on F^2
Refinement program	SHELXL-2014/7 (Sheldrick, 2014)
Function minimized	$\Sigma\, w(F_o^2 - F_c^2)^2$
Data / restraints / parameters	5533 / 0 / 270
Goodness-of-fit on F^2	1.025
Final R indices	4391 data; I>2σ(I) R1 = 0.0377, wR2 = 0.0930
	all data R1 = 0.0553, wR2 = 0.1018
Weighting scheme	$w=1/[\sigma^2(F_o^2)+(0.0492P)^2+0.7375P]$ where $P=(F_o^2+2F_c^2)/3$
Largest diff. peak and hole	0.415 and -0.249 $eÅ^{-3}$
R.M.S. deviation from mean	0.056 $eÅ^{-3}$

An orange needle-like specimen of $C_{23}H_{32}ClN_7O_3$, approximate dimensions 0.063 mm x 0.106 mm x 0.444 mm, was used for the X-ray crystallographic analysis. The X-ray intensity data were measured. The total exposure time was 27.95 hours. The frames were integrated with the Bruker SAINT software package using a narrow-frame algorithm. The integration of the data using a triclinic unit cell yielded a total of 33026 reflections to a maximum θ angle of 27.51° (0.77 Å resolution), of which 5737 were independent (average redundancy 5.757, completeness = 99.9%, R_{int} = 5.62%, R_{sig} = 4.66%) and 4184 (72.93%) were greater than $2\sigma(F^2)$. The final cell constants of a = 8.9177(2) Å, b = 9.9120(3) Å, c = 15.2783(4) Å, α = 99.227(2)°, β = 90.593(2)°, γ = 109.891(2)°, volume = 1250.42(6) $Å^3$, are based upon the refinement of the XYZ-centroids of 6854 reflections above 20 σ(I) with 5.333° < 2θ < 53.95°. Data were corrected for absorption effects using the multi-scan method (SADABS). The ratio of minimum to maximum apparent transmission was 0.912. The calculated minimum and maximum transmission coefficients (based on crystal size) are 0.9200 and 0.9880. The final anisotropic full-matrix least-squares refinement on F^2 with 329 variables converged at R1 = 4.06%, for the observed data and wR2 = 10.05% for all data. The goodness-of-fit was 1.008. The largest peak in the final difference electron density synthesis was 0.386 $e^-/Å^3$ and the largest hole was -0.218 $e^-/Å^3$ with an RMS deviation of 0.053 $e^-/Å^3$. On the basis of the final model, the calculated density was 1.301 g/cm^3 and F(000), 520 e^-.

Table 3. Sample and crystal data for carbocation sample.

Chemical formula	$C_{23}H_{32}ClN_7O_3$	
Formula weight	490.00 g/mol	
Temperature	100(2) K	
Wavelength	0.71073 Å	
Crystal size	0.063 x 0.106 x 0.444 mm	
Crystal habit	orange needle	
Crystal system	triclinic	
Space group	P -1	
Unit cell dimensions	a = 8.9177(2) Å	
	b = 9.9120(3) Å	α = 99.227(2)°
	c = 15.2783(4) Å	β = 90.593(2)°
Volume	1250.42(6) Å^3	γ = 109.891(2)°
Z	2	
Density (calculated)	1.301 g/cm^3	
Absorption coefficient	0.191 mm^{-1}	
F(000)	520	

Table 4. Data collection and structure refinement for carbocation.

Theta range for data collection	2.22 to 27.51°	
Index ranges	-11<=h<=11, -12<=k<=12, -19<=l<=19	
Reflections collected	33026	
Independent reflections	5737 [R(int) = 0.0562]	
Coverage of independent reflections	99.9%	
Absorption correction	multi-scan	
Max. and min. transmission	0.9880 and 0.9200	
Refinement method	Full-matrix least-squares on F^2	
Refinement program	SHELXL-2014/7 (Sheldrick, 2014)	
Function minimized	$\Sigma\, w(F_o^2 - F_c^2)^2$	
Data / restraints / parameters	5737 / 0 / 329	
Goodness-of-fit on F^2	1.008	
Δ/σ_{max}	0.001	
Final R indices	4184 data; I>2σ(I)	R1 = 0.0406, wR2 = 0.0904
	all data	R1 = 0.0683, wR2 = 0.1005
Weighting scheme	$w=1/[\sigma^2(F_o^2)+(0.0452P)^2+0.4356P]$ where $P=(F_o^2+2F_c^2)/3$	
Largest diff. peak and hole	0.386 and -0.218 eÅ^{-3}	
R.M.S. deviation from mean	0.053 eÅ^{-3}	

Acknowledgements

Special thanks to the RFUMS-DePaul University Pilot Grant for funding this research project. Special thanks also go to our Rosalind Franklin University of Medicine and Science collaborators Dr. Shivaputra Patil and Dr. Gulam Waris. In addition, thanks to Dr. Roger Sommer, who obtained x-ray crystallography images for our compounds. Similarly, thanks to Aeshah Niyazi who aided in the RFUMS project. Finally, thanks to Dr. Kyle Grice who served as an invaluable advisor and guide in this project.

References

1) El-Serag, H.B. *Gastroenterology*, **2012**, *142*, 1264–1273.
2) Llovet, J. M.; Ricci, S.; Mazzaferro, V.; Hilgard, P.; Gane, E.; Blanc, J.-F.; de Oliveira, A. C.; Santoro, A.; Raoul, J.-L.; Forner, A.; Schwartz, M.; Porta, C.; Zeuzem, S.; Bolondi, L.; Greten, T. F.; Galle, P. R.; Seitz, J.-F.; Borbath, I.; Häussinger, D.; Giannaris, T.; Shan, M.; Moscovici, M.; Voliotis, D.; Bruix, J. *New England Journal of Medicine* **2008**, *359*, 2497–2499.
3) McQuitty, R. J. *Science Progress* **2014**, *97*, 1–19.
4) Kelland, L. *Nat. Rev. Cancer*, **2007**, *7*, 573–584.
5) Burger, A.; Double, J.; Newell, D. *European Journal of Cancer* **1997**, *33* (4), 638–644.
6) Trinajstić, N. *Tetrahedron Letters* **1968**, *9* (12), 1529–1532.
7) Niu, Z.; Boggs, J. E. *Journal of Molecular Structure: THEOCHEM* **1984**, *109* (3-4), 381–389.
8) Patil, R.; Ghosh, A.; Sun Cao, P.; Sommer, R. D.; Grice, K. A.; Waris, G.; Patil, S. *Bioorganic and Medicinal Chemistry Letters*, **2017**, *27*, 1129–1135.
9) M.J. Frisch, G.W. Trucks, H.B. Schlegel, G.E. Scuseria, M.A. Robb, J.R. Cheeseman, G. Scalmani, V. Barone, B. Mennucci, G.A. Petersson, H. Nakatsuji, M. Caricato, X. Li, H.P. Hratchian, A.F. Izmaylov, J. Bloino, G., Zheng, J.L. Sonnenberg, M. Hada, M. Ehara, K. Toyota, R. Fukuda, J. Hasegawa, M. Ishida, T. Nakajima, Y. Honda, O. Kitao, H. Nakai, T. Vreven, J.A. Montgomery, J.E. Peralta, F. Ogliaro, M. Bearpark, J.J. Heyd, E. Brothers, K.N. Kudin, V.N. Staroverov, R. Kobayashi, J. Normand, K. Raghavachari, A. Rendell, J.C. Burant, S.S. Iyengar, J. Tomasi, M. Cossi, N. Rega, J.M. Millam, M. Klene, J.E. Knox, J.B. Cross, V. Bakken, C. Adamo, J. Jaramillo, R. Gomperts, R.E. Stratmann, O. Yazyev, A.J. Austin, R. Cammi, C. Pomelli, J.W. Ochterski, R.L. Martin, K. Morokuma, V.G. Zakrzewski, G.A. Voth, P. Salvador, J.J. Dannenberg, S. Dapprich, A.D. Daniels, O. Farkas, J.B. Foresman, J.V. Ortiz, J. Cioslowski, D.J. Fox; *Gaussian 09*, **2009**.
10) R.D. Dennington, T.A. Keith, J.M. Millam; *Gaussian Inc.*, **2008**
11) P. Stephens, F. Devlin, C. Chabalowski, M.J. Frisch; *J. Phys. Chem.*, **1994**, *98*, pp. 11623–11627
12) A.D. Becke; *J. Chem. Phys.*, **1993**, *98*, pp. 5648–5652
13) C. Lee, W. Yang, R.G. Parr; *Phys. Rev. B*, **1988**, *37*, p. 785
14) S.H. Vosko, L. Wilk, M. Nusair; *Can. J. Phys.*, **1980**, *58*, pp. 1200–1211
15) M.J. Frisch, J.A. Pople, J.S. Binkley; *J. Chem. Phys.*, **1984**, 80, pp. 3265–3269